

## Flexible graphene based microwave attenuators

This content has been downloaded from IOPscience. Please scroll down to see the full text.

2015 Nanotechnology 26 055201

(<http://iopscience.iop.org/0957-4484/26/5/055201>)

View [the table of contents for this issue](#), or go to the [journal homepage](#) for more

Download details:

IP Address: 165.132.143.236

This content was downloaded on 23/02/2015 at 02:57

Please note that [terms and conditions apply](#).

# Flexible graphene based microwave attenuators

Kisik Byun<sup>1</sup>, Yong Ju Park<sup>1</sup>, Jong-Hyun Ahn and Byung-Wook Min

School of Electrical and Electronic Engineering, Yonsei University, Sinchon-dong, Seodaemun-gu, Seoul 120-749, Korea

E-mail: [bmin@yonsei.ac.kr](mailto:bmin@yonsei.ac.kr)

Received 20 September 2014, revised 11 November 2014

Accepted for publication 8 December 2014

Published 15 January 2015



CrossMark

## Abstract

We demonstrate flexible 3 dB and 6 dB microwave attenuators using multilayer graphene grown by the chemical vapor deposition method. On the basis of the characterized results of multilayer graphene and graphene–Au ohmic contacts, the graphene attenuators are designed and measured. The flexible graphene-based attenuators have 3 dB and 6 dB attenuation with a return loss of less than  $-15$  dB at higher than 5 GHz. The devices have shown durability in a bending cycling test of 100 times. The circuit model of the attenuator based on the characterized results matches the experimental results well.

Keywords: microwave, graphene, attenuator, flexible electronics

(Some figures may appear in colour only in the online journal)

## Introduction

Flexible microwave systems have been dynamically developed because of various advantages: they are lightweight, bendable, portable, and inexpensive to manufacture [1, 2]. Although many kinds of research have been proposed [3–7], few flexible attenuators have been reported. Flexible attenuators with constant attenuation are required in various flexible microwave systems to control the signal power level. Therefore, flexible attenuators, as components of flexible circuits, need to be developed for flexible microwave systems. Conventional thin-film resistors such as nichrome (NiCr), copper-nickel (CuNi), and tantalum nitride (TaN) are used for portable terminal attenuators [8–11]. However, these materials are of limited utility for flexible electronics due to their intrinsic mechanical properties. As an alternative, atom-thick graphene is a highly promising candidate material for flexible attenuator systems because graphene not only has splendid mechanical properties but also tunable resistance through the use of multilayer stacks, different metal catalyst films, and electrostatic/chemical doping [12–16]. Furthermore, graphene-based attenuators possess greater power handling capability than conventional resistive layers due to their high breakdown-current density [17, 18]. In this paper, we

demonstrate a flexible and practical microwave attenuator fabricated using multilayer graphene on a PET substrate. The attenuator was designed based on experimental results involving RF transmission properties and graphene–Au ohmic contact properties. The flexible graphene attenuator shows 3 dB and 6 dB attenuation, which matches simulation results, and excellent mechanical flexibility.

## Experimental setup

Figure 1(a) is a photograph of a test structure to characterize the graphene layer and graphene–Au ohmic contact [19]. The characteristics of the graphene layer, graphene–Au ohmic contact, and coplanar waveguide (CPW) transmission line need to be considered to optimize the design of the attenuator. To analyze their effects, we built the test structure with multilayer graphene on Au CPW transmission lines with a  $90\ \mu\text{m}$  center line and a  $6\ \mu\text{m}$  gap, which have a characteristic impedance of  $50\ \Omega$ , on  $188\ \mu\text{m}$ -thick polyethylene terephthalate (PET) substrate. In the first step, the PET substrate was pre-annealed at  $120\ ^\circ\text{C}$  for 1 h to avoid thermal expansion during the fabrication process. Ground (G)–signal (S)–ground (G) electrodes were formed on the PET substrate by thermal evaporation of Au metal (40 nm), with the liftoff pattern made by the photoresist. The transmission line was fabricated with a

<sup>1</sup> These authors contributed equally to this work.

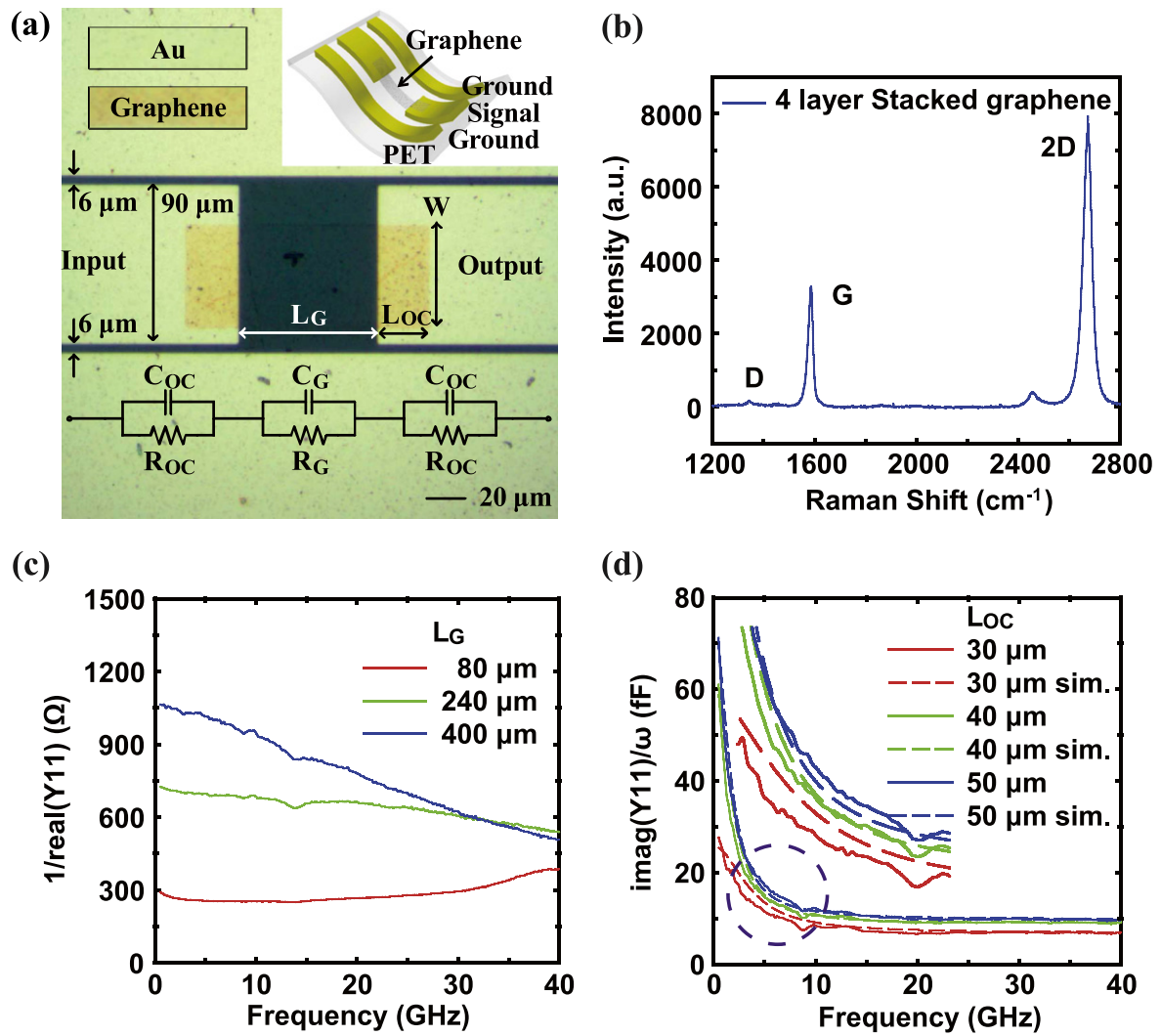


**Figure 1.** (a) Photograph and lumped circuit model of the test structure to characterize multilayer graphene and graphene–Au ohmic contacts on 188 μm PET substrate. (b) Raman spectrum of four-layer stacked graphene. (c) Measured  $1/\text{real}(Y_{11})$  of the test structure with different graphene lengths ( $L_G$ ). (d) Measured  $\text{imag}(Y_{11})/\omega$  of the test structure with different lengths of the graphene–Au ohmic contact ( $L_{OC}$ ).

40 nm Au layer to achieve good flexibility, and the Au transmission lines were designed to be very short to minimize the loss of the GSG electrodes because transmission lines with a thin metal layer have a high insertion loss. Since the Au thickness is thinner than the skin depth in the designed frequency range (377 nm at 40 GHz), this transmission line has the advantage of less loss variation over the frequency range. We used four-layer graphene to achieve suitable sheet resistance on the PET substrate [20]. The graphene was synthesized on a Cu foil by a typical chemical vapor deposition technique [13]. The graphene layer was wet-etched with 0.1 M of ammonium persulfate (APS) and transferred onto the Au–PET substrate using a polymethyl methacrylate (PMMA) supporting layer. The top PMMA was removed by acetone after the PMMA–graphene–Au–PET sample was dried. By repeating this simple wet transfer process, high-quality four-layer graphene was achieved. The pattern of multilayer graphene was defined by photolithography and O<sub>2</sub> plasma [21]. Figure 1(b) shows the Raman spectrum of four-

layer stacked graphene. The intensity ratio of G and the 2D peak indicate properties of typical four-layer stacked graphene: the upper and lower layers are randomly oriented, and the low intensity of the D peak indicates low defect density of the graphene [13].

## Results and discussion

To characterize the RF transmission properties of multilayer graphene, the input and output CPW transmission lines are connected to the multilayer graphene, which has a length and width of  $L_G$  and  $W$ , respectively. The equivalent lumped circuit model of the test structure is shown in the inset of figure 1(a).  $C_{OC}$  and  $R_{OC}$  are the capacitance and resistance of the ohmic contact,  $R_G$  is the resistance where only the graphene layer exists (not overlapping the Au electrode), and  $C_G$  is the parasitic capacitance between CPW transmission lines of the test structure. From the circuit model,  $Y_{11}$  of the two-

**Table 1.** Parameters of the graphene test structure model.

W ( $\mu\text{m}$ )	L <sub>OC</sub> ( $\mu\text{m}$ )	R <sub>G</sub> ( $\Omega$ )	C <sub>G</sub> (fF)	R <sub>OC</sub> ( $\Omega$ )	C <sub>OC</sub> (pF)
80	30	215	7	12	4.0
80	40	215	9	17	6.0
80	50	215	10	19	6.0

port test structure can be expressed as

$$\begin{aligned}
Y11 = & \left[ (R_G + 2R_{OC}) \right. \\
& + \omega^2 R_{OC} R_G (C_{OC}^2 R_{OC} + 2C_G^2 R_G) \\
& + j[2\omega C_{OC} R_{OC}^2 + \omega C_G R_G^2 \\
& + 2\omega^3 C_{OC} C_G R_{OC}^2 R_G^2 (C_G + C_{OC}/2)] \Big] / \\
& \left( (R_G + 2R_{OC})^2 + 4\omega^2 R_{OC}^2 R_G^2 (C_G + C_{OC}/2)^2 \right). \quad (1)
\end{aligned}$$

To find the graphene resistance in the form of sheet resistance, L<sub>G</sub> is varied from 80  $\mu\text{m}$  to 400  $\mu\text{m}$ , whereas W and L<sub>OC</sub> are fixed at 80  $\mu\text{m}$  and 10  $\mu\text{m}$ , respectively. Since the length and width are defined as the number of resistive squares, the graphene size is varied from one to five squares. The two-port S-parameters of the test structures are measured from 0.5 GHz to 40 GHz and transformed into the Y-parameters [22]. Since, from equation (1),

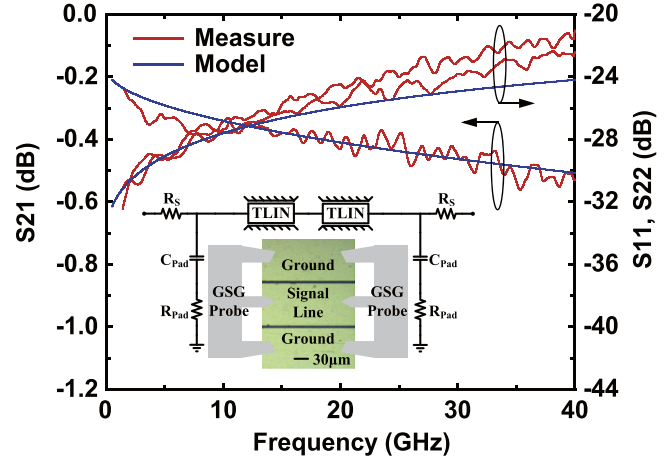
$$\frac{1}{\text{real}(Y11)} \Big|_{\omega \rightarrow 0} = R_G + 2R_{OC} \quad (2)$$

and R<sub>OC</sub> is fixed, R<sub>G</sub> can be found from the 1/real(Y11)| <sub>$\omega \rightarrow 0$</sub>  differences between the test structures with various L<sub>G</sub>. Figure 1(c) shows the measured 1/real(Y11), and the sheet resistance of the multilayer graphene can be estimated to be 215  $\Omega \text{sq}^{-1}$  from the measured results at the lowest frequency of 0.5 GHz.

To characterize the graphene–Au ohmic contact, the graphene–Au overlap length (L<sub>OC</sub>) is maintained in the range 30  $\mu\text{m}$  to 50  $\mu\text{m}$ , whereas L<sub>G</sub> and W are maintained at 80  $\mu\text{m}$ . Figure 1(d) shows the imag(Y11)/ $\omega$  for L<sub>OC</sub> of 30, 40, and 50  $\mu\text{m}$ . Since C<sub>OC</sub> is much larger than the parasitic capacitance C<sub>G</sub>, from equation (1) C<sub>G</sub> can be derived from

$$\frac{\text{imag}(Y11)}{\omega} \Big|_{\omega \rightarrow \infty} = \frac{1}{\frac{2}{C_{OC}} + \frac{1}{C_G}} \cong C_G. \quad (3)$$

The imag(Y11)/ $\omega$  lines converge to a fixed capacitance after 10 GHz, which means that 40 GHz is a high enough frequency for  $\omega \rightarrow \infty$ , and C<sub>G</sub> can be estimated to be 7~10 fF depending on L<sub>G</sub>. R<sub>OC</sub> and C<sub>OC</sub> define the slope of the imag(Y11)/ $\omega$  convergence, and the value of R<sub>OC</sub> and C<sub>OC</sub> can be found by curve-fitting the imag(Y11)/ $\omega$  lines. The model parameters of the fitted curve are R<sub>OC</sub>=11~19  $\Omega$  and C<sub>OC</sub>=4000~6000 fF for L<sub>OC</sub>=30~50  $\mu\text{m}$ . The model parameters for the various L<sub>OC</sub> are summarized in table 1. The series impedance of the ohmic contact is the parallel combination of R<sub>OC</sub> and 1/j $\omega$ C<sub>OC</sub>, and the impedance of the ohmic

**Figure 2.** Measured and modeled S-parameters of a 200  $\mu\text{m}$  CPW transmission line with GSG probe contact resistance and discontinuity.**Table 2.** Parameters of the line model at 30 GHz.

R <sub>S</sub> ( $\Omega$ )	R <sub>Ppad</sub> ( $\Omega$ )	C <sub>Ppad</sub> (fF)	Z <sub>0</sub> ( $\Omega$ )	$\epsilon_{\text{eff}}$	$\alpha$ (dB mm <sup>-1</sup> )
1	10	1	50	3.0	3

contact is around 4  $\Omega$  at 5 GHz and becomes even lower at higher frequency. Therefore, graphene-based microwave circuits with 50  $\Omega$  port impedance are not affected much by ohmic contact impedance at higher than 5 GHz as long as the ohmic contact is large enough (80  $\times$  30  $\mu\text{m}^2$ ). Therefore, we designed the microwave attenuators for frequencies higher than 5 GHz.

Figure 2 shows the measured S-parameters of a 200  $\mu\text{m}$  CPW transmission line. From the experimental result, we obtained the transmission line characteristics and the discontinuity of the GSG probe contacts through curve fitting in order to conduct more accurate attenuator modeling. C<sub>Ppad</sub> and R<sub>Ppad</sub> are due to the pad parasitics of the GSG contacts, R<sub>S</sub> is the probe contact resistance, and TLIN is the general model of transmission line. Table 2 summarizes the modeled values, where Z,  $\epsilon_{\text{eff}}$ , and  $\alpha$  are the characteristic impedance, effective relative dielectric constant, and line loss of TLIN at 30 GHz, respectively. The characteristic impedance Z<sub>0</sub> is 50  $\Omega$ , and  $\epsilon_{\text{eff}}$  (3.0) is smaller than  $\epsilon_{\text{PET}}$  (3.4) since the transmission line is CPW, where some fields from the conductor exist in air. As the frequency increases, the transmission line loss increases due to the finite conductivity of 40 nm-thick Au. The loss is about 1.7 dB mm<sup>-1</sup> at 10 GHz and 3 dB mm<sup>-1</sup> at 30 GHz.

The matched microwave attenuator can be made with three resistors in  $\Pi$  or T configurations, and the resistor values depend on the attenuation levels. For the  $\Pi$ -type attenuator design in figure 3(a), the values of resistances (R<sub>1</sub>, R<sub>2</sub>) can be determined from the port impedance (Z<sub>0</sub>). The R<sub>1</sub> and R<sub>2</sub> values of the A-dB  $\Pi$  attenuator can be calculated as

$$R_1 = \frac{Z_0}{2} \times (10^{A/10} - 1) \times 10^{-A/20}, \quad (4)$$

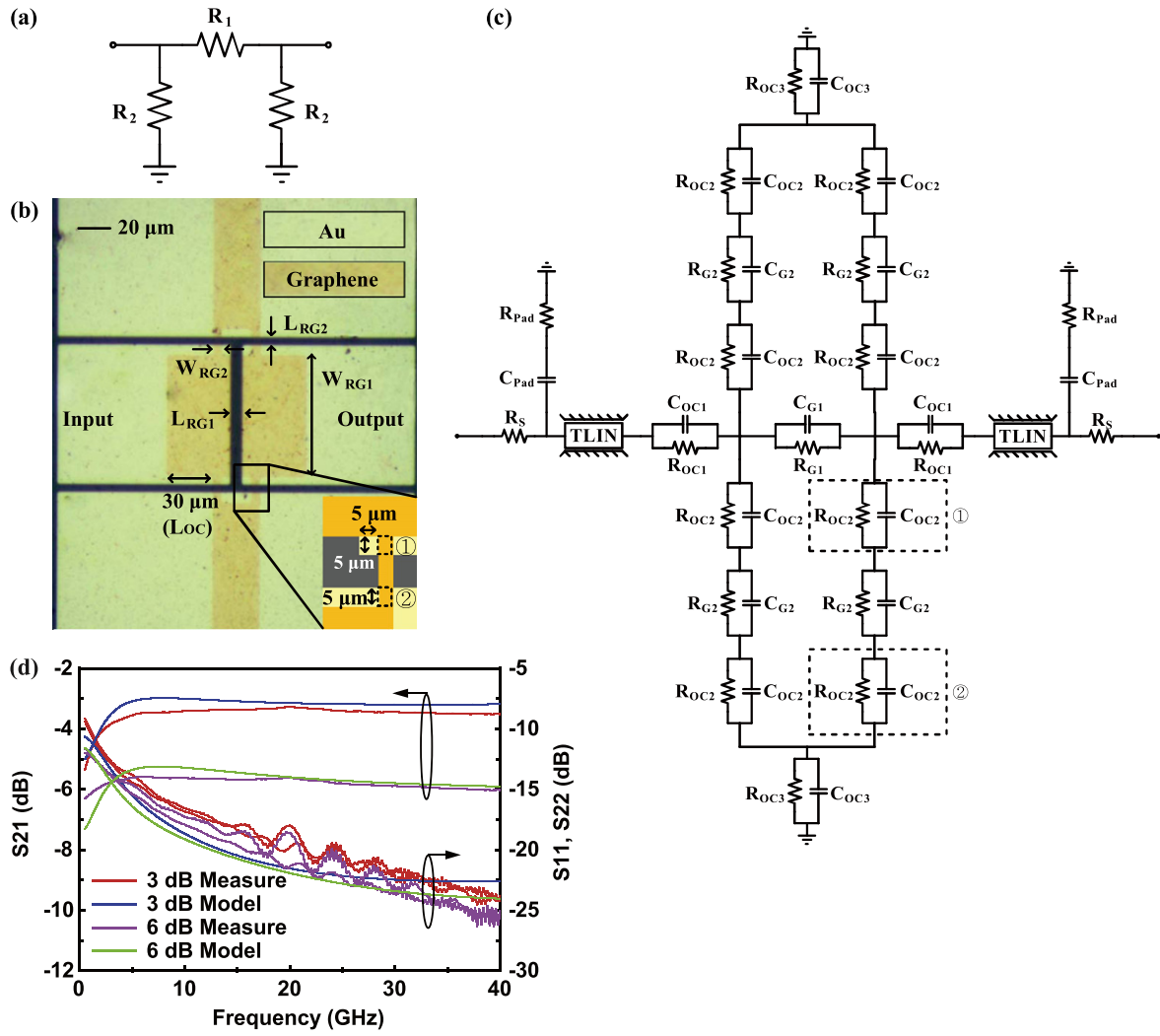


**Figure 3.** (a) Structure of the  $II$ -type microwave attenuator. (b) Photograph of the graphene attenuator. (c) Circuit model of the graphene attenuator cascaded with the modeled ohmic contact and graphene layer and CPW transmission line. (d) Measured and modeled S-parameters of the 3 dB and 6 dB graphene attenuators.

$$R_2 = \frac{Z_0 \times (10^{A/10} - 1)}{10^{A/10} - 2 \times 10^{A/20} + 1}. \quad (5)$$

Because the CPW transmission line has ground planes on both sides of the signal line,  $R_2$  is divided into two  $R_{G2}$ , which are connected to two ground planes. For the 3 dB attenuator, it can be calculated that  $R_{G1} = 17.6 \Omega$  and  $R_{G2} = 584 \Omega$ , and the 6 dB attenuator should have  $R_{G1} = 37.4 \Omega$  and  $R_{G2} = 302 \Omega$ . We designed the dimensions of  $R_{G1}$  and  $R_{G2}$  ( $W_{RG1}$ ,  $L_{RG1}$ ,  $W_{RG2}$ , and  $L_{RG2}$ ) using the characterized sheet resistance of graphene layers, and they are summarized in table 3. The graphene resistors are integrated into the  $50 \Omega$  CPW transmission line as shown in figure 3(b). The graphene layer and Au CPW transmission lines have a  $5 \mu\text{m}$  margin in preparation for fabrication misalignment, as shown in the inset of figure 3(b). We simulated the graphene attenuator with a commercial electromagnetic and circuit simulator using previously characterized results (graphene–Au ohmic contact and line model) as shown in figure 3(c).

**Table 3.** Design parameters of the graphene attenuator.

	$R_{G1} (\Omega)$	$W_{R1} (\mu\text{m})$	$L_{R1} (\mu\text{m})$	$R_{G2} (\Omega)$	$W_{R2} (\mu\text{m})$	$L_{R2} (\mu\text{m})$
3 dB	17.6	80	4.5	584	3	6
6 dB	37.4	80	8.5	302	6.5	6

Figure 3(d) shows the measured and modeled S-parameters of the 3 dB and 6 dB attenuators. They have 3 dB and 6 dB attenuation ( $S_{21}$ ), and the input and output return loss ( $S_{11}$ ,  $S_{22}$ ) is less than  $-15$  dB at higher than 5 GHz. The graphene attenuators show the designed attenuation and low return loss at frequencies higher than 5 GHz because these attenuators are not affected by the ohmic contact resistance due to the ohmic contact capacitance. Table 4 summarizes the circuit model parameters of the attenuators.  $R_{G1}$  and  $R_{G2}$  have the same values as those calculated by equations (4) and (5).  $L_{OC}$  of the attenuators is  $30 \mu\text{m}$ , and therefore  $R_{OC1}$ ,  $R_{OC3}$ ,  $C_{OC1}$ , and  $C_{OC3}$  have reasonable values compared with the previously characterized results (table 1).  $R_{OC2}$  and  $C_{OC2}$  are

**Table 4.** Parameters of the graphene attenuator model.

	$R_{G1}$ ( $\Omega$ )	$C_{G1}$ (fF)	$R_{G2}$ ( $\Omega$ )	$C_{G2}$ (fF)	$R_{OC1}$ ( $\Omega$ )	$C_{OC1}$ (fF)	$R_{OC2}$ ( $\Omega$ )	$C_{OC2}$ (fF)	$R_{OC3}$ ( $\Omega$ )	$C_{OC3}$ (fF)
3 dB	17	100	585	1			300	100		
6 dB	32.5	20	300	1	20	4000	90	170	14	4500

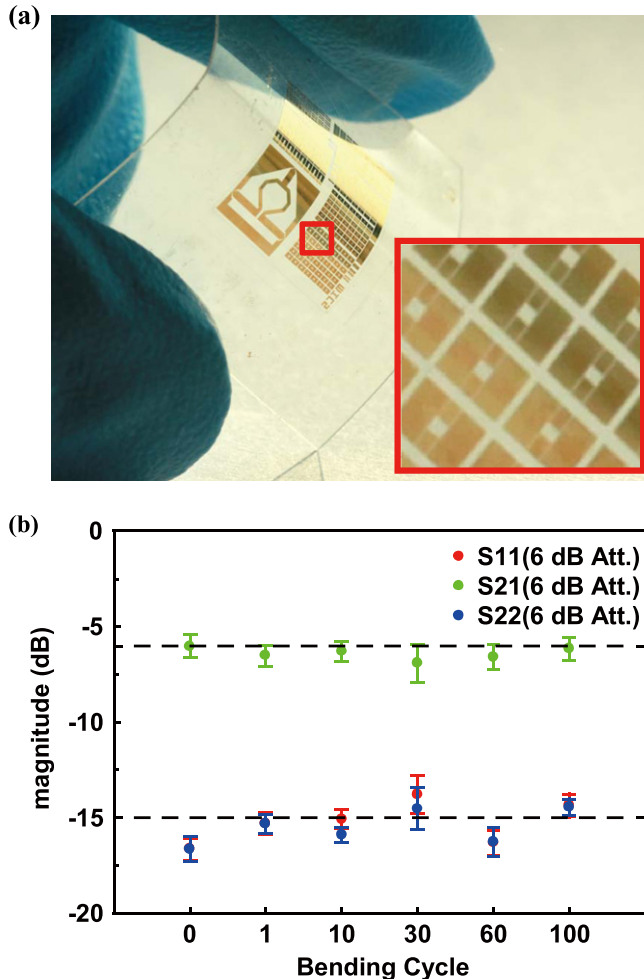


**Figure 4.** (a) Photograph of an array of devices on a PET substrate. (b) The variations of attenuation and return loss at 10 GHz and bending radius of 5 mm.

the model of short ohmic contact lines (ⓐ, ⓑ in figure 3(b)). These 5  $\mu\text{m}$ -long ohmic contacts are prepared as a margin for fabrication misalignment.

The mechanical flexibility of the graphene-based attenuator on a PET substrate was studied by characterizing the device performance during repeated bending. The device was repeatedly bent along directions parallel to the attenuator channel length. Figure 4(a) shows an array of devices on the PET substrate and the magnified image of the attenuator arrays (inset). Figure 4(b) shows the variations in attenuation and return loss at 10 GHz after repeated bending to a radius of 5 mm, which corresponds to a tensile strain of 2%. The devices exhibit stable operation without significant change in attenuation and return loss (2.3 dB) even after 100 bending

cycles. The bending tests demonstrate the stable and reliable operation of the graphene-based attenuators.

## Conclusion

In conclusion, we designed and fabricated flexible graphene-based attenuators having 3 dB and 6 dB attenuation for applications at higher than 5 GHz. The flexible graphene-based attenuators are well matched, and the return loss is less than  $-15$  dB. The graphene-based attenuators show mechanical stability and stable attenuation along with the intrinsically flexible characteristics of graphene. We also confirmed that circuit models of the flexible graphene attenuators accurately predict the performance of the device. These modeled characteristics can provide a route to developing various practical flexible microwave components such as variable attenuators and power dividers.

## Acknowledgments

This research was supported by the Basic Science Research Program through the National Research Foundation of Korea (NRF), funded by the Ministry of Science, ICT, & Future Planning (2014R1A1A1004614). Also, this research was financially supported by the ‘Sensitivity touch platform development and new industrialization support program’ through the Ministry of Knowledge Economy (MKE) and the Korea Institute for Advancement of Technology (KIAT).

## References

- [1] Wong W S and Salleo A 2009 *Flexible Electronics: Materials and Applications* (New York: Springer)
- [2] Kim D-H *et al* 2011 Epidermal electronics *Science* **333** 838–43
- [3] Lee S-K, Kabir S H, Sharma B K, Kim B J, Cho J H and Ahn J-H 2014 Photo-patternable ion gel-gated graphene transistors and inverters on plastic *Nanotechnology* **25** 014002
- [4] Nomura K, Ohta H, Takagi A, Kamiya T, Hirano M and Hosono H 2004 Room-temperature fabrication of transparent flexible thin-film transistors using amorphous oxide semiconductors *Nature* **432** 488–92
- [5] Rogers J A *et al* 2001 Paper-like electronic displays: large-area rubber-stamped plastic sheets of electronics and microencapsulated electrophoretic inks *Proc. Natl. Acad. Sci. USA* **98** 4835–40
- [6] Vaillancourt J *et al* 2008 All ink-jet-printed carbon nanotube thin-film transistor on a polyimide substrate with an ultrahigh operating frequency of over 5 GHz *Appl. Phys. Lett.* **93** 243301

- [7] Kim D-H, Ahn J-H, Kim H-S, Lee K J, Kim T-H, Yu C-J, Nuzzo R G and Rogers J A 2008 Complementary logic gates and ring oscillators on plastic substrates by use of printed ribbons of single-crystalline silicon *IEEE Electron Device Lett.* **29** 73
- [8] Cuong N D, Yoon S-G, Kim D-J and Kang B-D 2007 Ti(N) thin film resistors for 20 dB  $\Pi$ -type attenuator applications *Appl. Phys. Lett.* **90** 183506
- [9] Vinayak S, Vyas H P, Muraleedharan K and Vankar V D 2006 Ni-Cr thin film resistor fabrication for GaAs monolithic microwave integrated circuits *Thin Solid Films* **514** 52–7
- [10] Hur S-G, Kim D-J, Kang B-D and Yoon S-G 2005 The Structural and electrical properties of CuNi thin-film resistors grown on AlN substrates for  $\Pi$ -type attenuator application *J. Electrochem. Soc.* **152** G472–6
- [11] Cuong N D, Kim D-J, Kang B-D and Yoon S-G 2006 Structural and electrical characterization of tantalum nitride thin film resistors deposited on AlN substrates for  $\pi$ -type attenuator applications *Mater. Sci. Eng.: B* **135** 162–5
- [12] Lee S-K, Kim B J, Jang H, Yoon S C, Lee C, Hong B H, Rogers J A, Cho J H and Ahn J-H 2011 Stretchable graphene transistors with printed dielectrics and gate electrodes *Nano Lett.* **11** 4642–6
- [13] Bae S *et al* 2010 Roll-to-roll production of 30-inch graphene films for transparent electrodes *Nature Nanotechnol.* **5** 574–8
- [14] Park J-U, Nam S, Lee M-S and Lieber C M 2012 Synthesis of monolithic graphene-graphite integrated electronics *Nature Mater.* **11** 120–5
- [15] Bae S-H, Kahya O, Sharma B K, Kwon J, Cho H J, Ozyilmaz B and Ahn J-H 2013 Graphene-P (VDF-TrFE) multilayer film for flexible applications *ACS Nano* **7** 3130–8
- [16] Han T-H, Lee Y, Choi M-R, Woo S-H, Bae S-H, Hong B H, Ahn J-H and Lee T-W 2012 Extremely efficient flexible organic light-emitting diodes with modified graphene anode *Nature Photon.* **6** 105–10
- [17] Lee K-J, Chandrakasan A P and Kong J 2011 Breakdown current density of CVD-grown multilayer graphene interconnects *IEEE Electron Device Lett.* **32** 557–9
- [18] Thomson F S, Mansour R R, Ye S and Jolley W 1998 Current density and power handling of high-temperature superconductive thin film resonators and filters *IEEE Trans. Appl. Supercond.* **8** 84–93
- [19] Moon S, Jung K, Park K, Kim H J, Lee C-W, Baik C-W and Kim J M 2010 Intrinsic high-frequency characteristics of graphene layers *New J. Phys.* **12** 113031
- [20] Kim K, Bae S-H, Toh C T, Kim H, Cho J H, Whang D, Lee T-W, Ozyilmaz B and Ahn J-H 2014 Ultrathin organic solar cells with graphene doped by ferroelectric polarization *ACS Appl. Mater. Interfaces* **6** 3299–304
- [21] Lee S-K, Jang H Y, Jang S, Choi E, Hong B H, Lee J, Park S and Ahn J-H 2012 All graphene-based thin film transistors on flexible plastic substrates *Nano Lett.* **12** 3472–6
- [22] Pozar D M 2011 *Microwave Engineering* 4th edn (Hoboken, NJ: Wiley)